Supporting Information

Ultrahigh-Field ^{25}Mg NMR and DFT Study of Magnesium Borate Minerals

Bing Zhou,[1] Alexandra Faucher,[2†] Robert Laskowski,[3] Victor V. Terskikh,[4] Scott Kroeker,[5] Wei Sun,[6,7] Jinru Lin,[6] Jin-Xiao Mi,[7] Vladimir K. Michaelis[2*] and Yuanming Pan[6*]

1. College of Materials Science and Engineering, Tongji University, Shanghai 21000, China
2. Department of Chemistry, University of Alberta, Edmonton, Alberta T6G 2G2, Canada
3. Institute of High Performance Computing, A*STAR, 1 Fusionopolis Way, #16-16, Connexis, Singapore 138632
4. Department of Chemistry, University of Ottawa, Ottawa, Ontario K1N 6N5 Canada
5. Department of Chemistry, University of Manitoba, Winnipeg, Manitoba R3T 2N2, Canada
6. Department of Geological Sciences, University of Saskatchewan, Saskatoon, Saskatchewan S7N 5E2, Canada
7. Fujian Provincial Key Laboratory of Advanced Materials, Department of Materials Science and Engineering, College of Materials, Xiamen University, Xiamen 361005, Fujian Province, China

[†]Current address: Bernal Institute, University of Limerick, Limerick, Republic of Ireland

[§]BZ and AF contributed equally

[*]Corresponding authors: Vladimir Michaelis (vladimir.michaelis@ualberta.ca) and Yuanming Pan (yuanming.pan@usask.ca)

Table of Contents

Table S1. Acquisition parameters used in ^{25}Mg NMR experiments at B_0 = 21.1 T.

compound	pulse sequence	no. of echoes	spikelet separation / kHz	recycle delay / s	number of transients	total expt. time / hrs
kotoite	quad echo	-	-	30	1792	15
suanite	quad echo	-	-	30	2176	18
grandidierite	quad echo	-	-	10	6144	17
MgB_4O_7	WURST-QCPMG	128	4	60	1024	17
hungchaoite	Bloch pulse	-	-	10	296	0.8
szaibelyite	quad echo	-	-	5	10 240	14
fluoborite	quad echo	-	-	30	2048	17
$Mg_3B_7O_{13}Br$	quad echo	-	-	4	98304	108
	WURST-QCPMG	96	4	4	4096	5
boracite	quad echo	-	-	2	27648	15
	WURST-QCPMG	64	5	1	3072	0.9

Table S2. DFT calculated ^{25}Mg NMR magnetic shielding parameters.

		Calculated Magnetic Shielding Parameters		
Formula	Mineral Name	σ_{iso} / ppm	Ω / ppm	κ
$Mg_3B_2O_6$	kotoite	551.9	23.91	−0.187
		561.7	5.68	0.912
$Mg_2B_2O_5$	suanite	558.8	13.42	−0.072
		559.0	14.89	−0.403
$MgAlBO_4$	sinhalite	557.1	9.43	−0.784
$MgAl_3BSiO_9$	grandidierite	543.8	40.36	−0.560
MgB_4O_7		548.7	25.03	0.128
$MgBO_2(OH)$	szaibelyite	557.7	20.99	0.282
		552.1	12.18	0.131
$MgB_4O_5(OH)_4{\cdot}3H_2O$	hungchaoite	563.1	4.27	0.093
$MgB_3O_3(OH)_5{\cdot}5H_2O$	indierite	562.0	12.55	−0.233
$MgB_3O_3(OH)_5{\cdot}5H_2O$	kurnakovite	558.4	12.21	0.592
$Mg_3(BO_3)(OH)_3$	hydroxylborite	546.6	17.03	0.572
$Mg_3(BO_3)F_3$	fluoborite	560.7	10.79	0.314
$Mg_3B_7O_{13}Cl$	boracite	555.7	20.20	−0.143
		555.9	20.00	−0.557
		554.3	21.29	−0.492
$Mg_3B_7O_{13}Br$		554.8	27.95	−1.000
MgO	periclase	534.9	0.00	1.000
$Mg(OH)_2$	brucite	550.8	14.69	−0.948
$MgAl_2O_4$	spinel	509.3	0.00	1.00

Table S3. Mg coordination number (CN) and longitudinal strain (LS) parameters

C.N.	Compound	$Mg\varphi_x$	r_0	LS
6		MgO_4Br_2	2.347	0.442
	brucite	$Mg(OH)_6$	2.099	0.002
	fluoborite	MgO_3F_3	2.051	0.053
	hungchaoite	$Mg(OH)(H_2O)_5$	2.080	0.014
	hydroxylborite	$MgO_3(OH)_3$	2.064	0.042
	indierite[b]	$MgO_2(H_2O)_4$	2.086	0.034
	kotoite	MgO_6	2.084	0.008
			2.110	0.050
	kurnakovite[b]	$MgO(H_2O)_5$	2.074	0.039
	sinhalite	MgO_6	2.092	0.055
	suanite	$Mg(1)O_6$	2.106	0.089
		$Mg(2)O_6$	2.090	0.023
	szaibelyite	$Mg(1)(O_5OH)$	2.090	0.042
		$Mg(2)(O_4(OH)_2)$	2.121	0.037
5	boracite	$Mg(1)O_4Cl$	2.160	0.332
		$Mg(2)O_4Cl$	2.158	0.408
		$Mg(3)O_4Cl$	2.150	0.422
	grandidierite	MgO_5	2.028	0.004
	MgB_4O_7	MgO_5	2.090	0.084
		MgO_6	2.210	0.220
4	spinel	MgO_4	1.926	0.000

φ: denoting the nearest neighbors such as O, OH, H_2O, F, Cl or Br.
r_0 = Average bond distance
LS: modified longitudinal strain

Table S4: Calculated results for ^{27}Al, ^{11}B and ^{29}Si in grandidierite using WIEN2k

Sites	$\sigma_{iso,}$ ppm	Ω, ppm	κ	$C_{Q,}$ MHz	η
Al(1)	544.84	10.98	0.185	3.35	0.66
Al(2)	544.48	23.67	0.395	7.57	0.89
Al(3)	511.80	32.72	0.993	-9.30	0.50
B	82.97	14.29	0.002	2.47	0.17
Si	425.67	17.73	-0.458	-	-

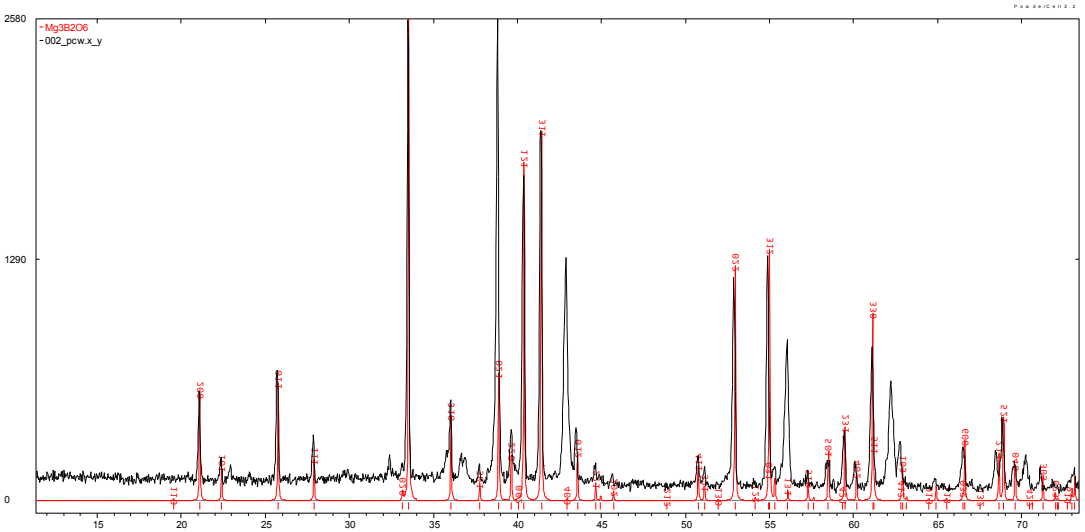

Figure S1. Experimental (black) and simulated (red) powder X-ray diffractograms for synthetic kotoite. Peaks unaccounted for in the simulation are due to the presence of MgO.

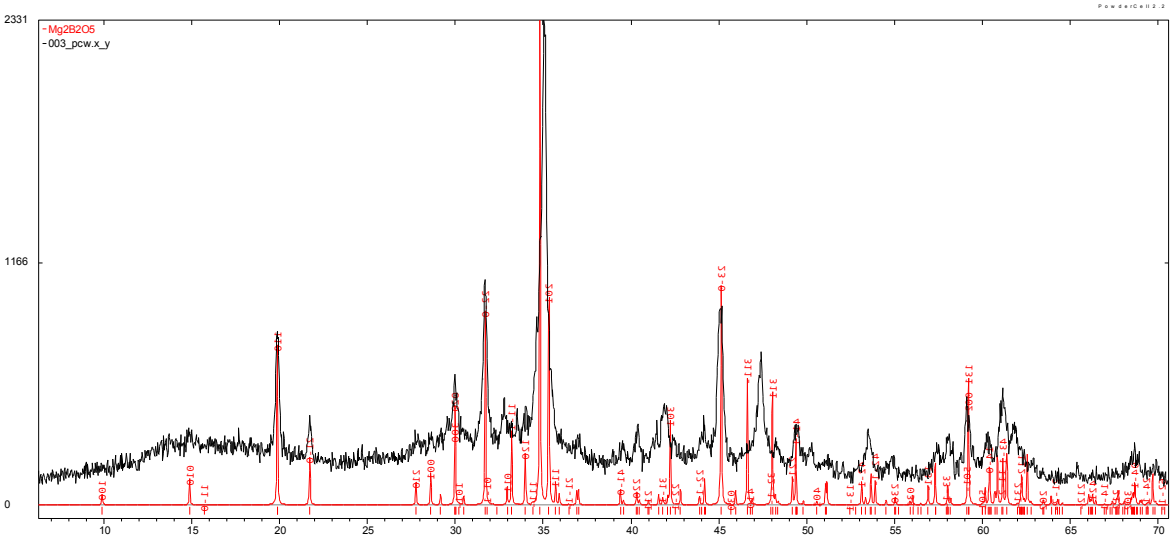

Figure S2. Experimental (black) and simulated (red) powder X-ray diffractograms for synthetic suanite.

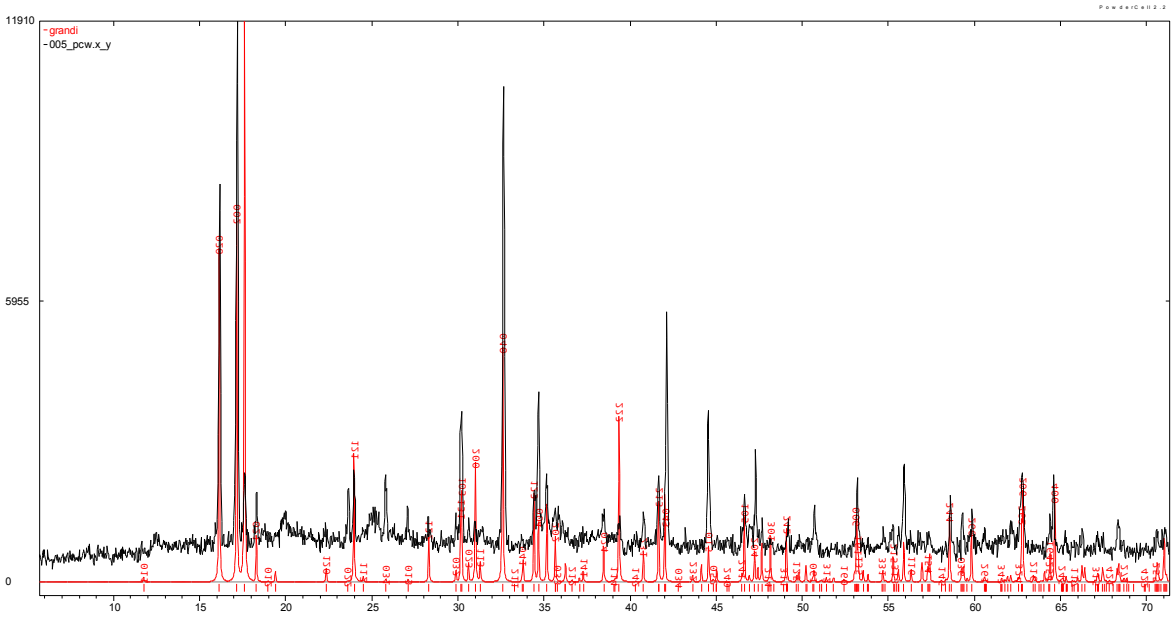

Figure S3. Experimental (black) and simulated (red) powder X-ray diffractograms for grandidierite sourced from Andrahomana, southern Madagascar.

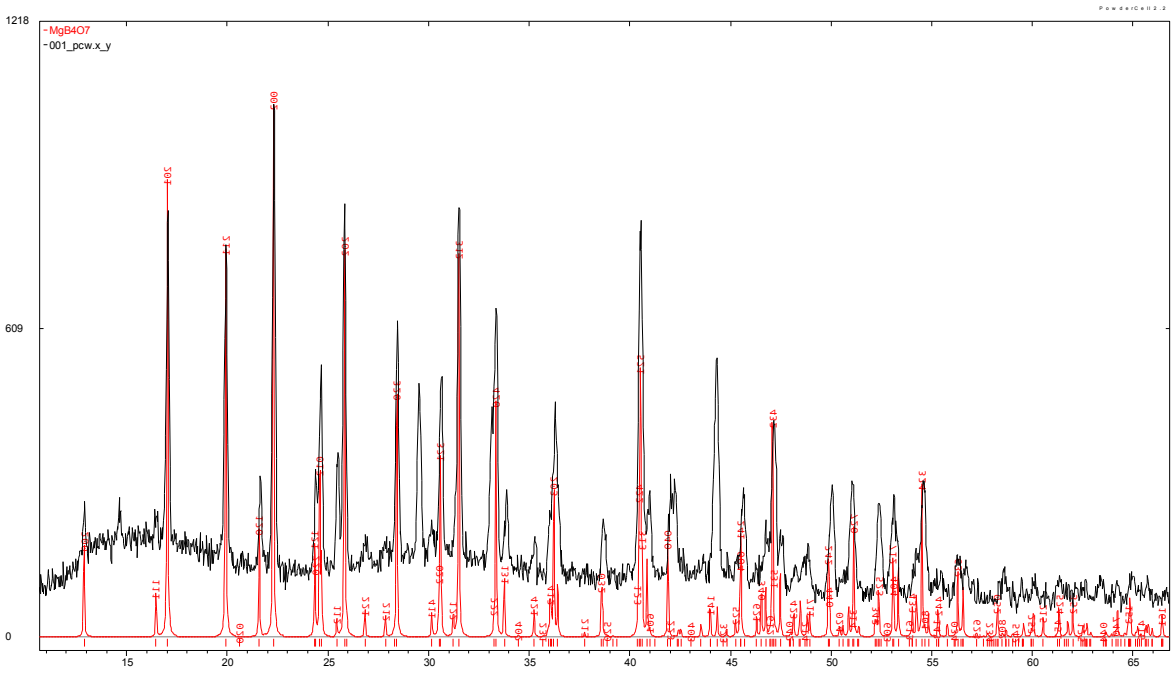

Figure S4. Experimental (black) and simulated (red) powder X-ray diffractograms for synthetic MgB_4O_7. Peaks unaccounted for in the simulation are due to the presence of MgO.

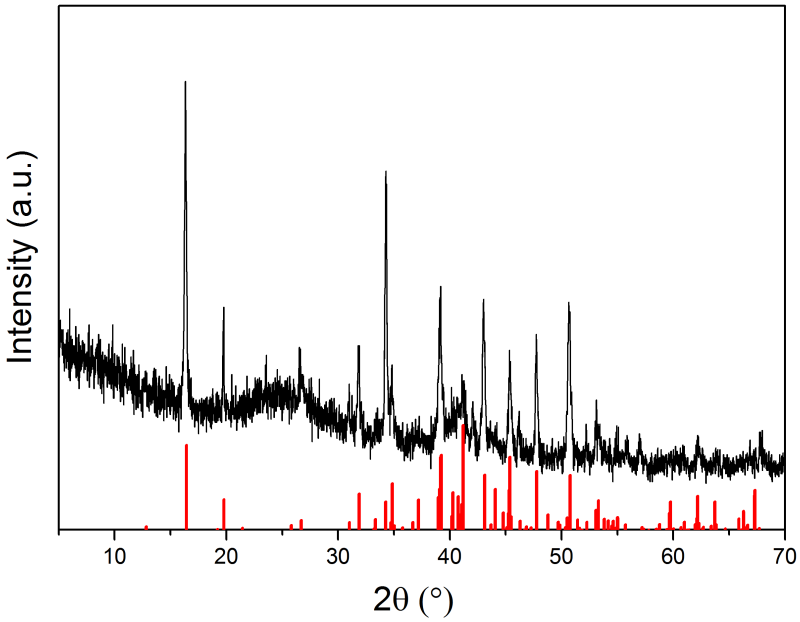

Figure S5. Experimental (black) powder X-ray diffractogram for hungchaoite. Red vertical bars are a simulated powder X-ray diffractogram generated from the crystal structure of hungchaoite (reference code: 98-000-6247, ICSD collection code: 10423; Ghose and Wan (1977) American Mineralogist, 62, 1135-1143).

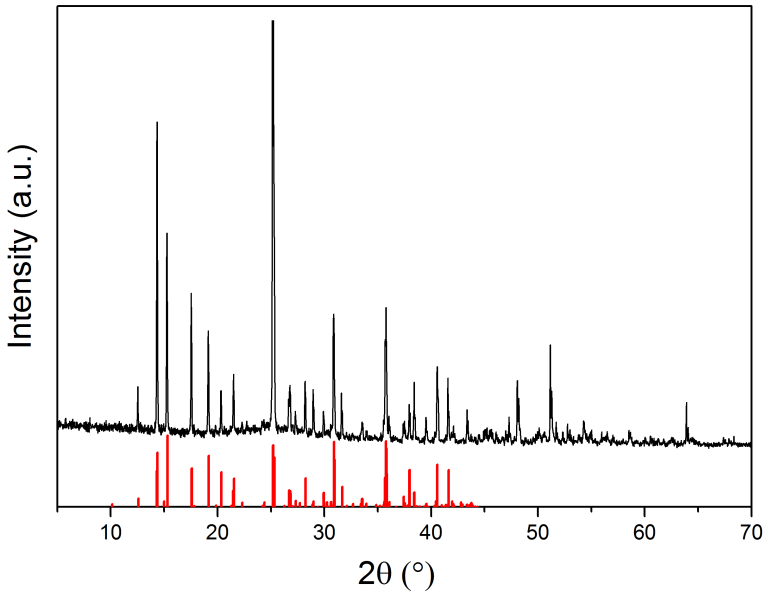

Figure S6. Experimental powder X-ray diffractogram for szaibelyite. Red vertical bars are a simulated powder X-ray diffractogram generated from the crystal structure of szaibelyite (reference code: 98-011-4075, ICSD code: 161275; Grice (2008) Canadian Mineralogist, 46, 671-677).

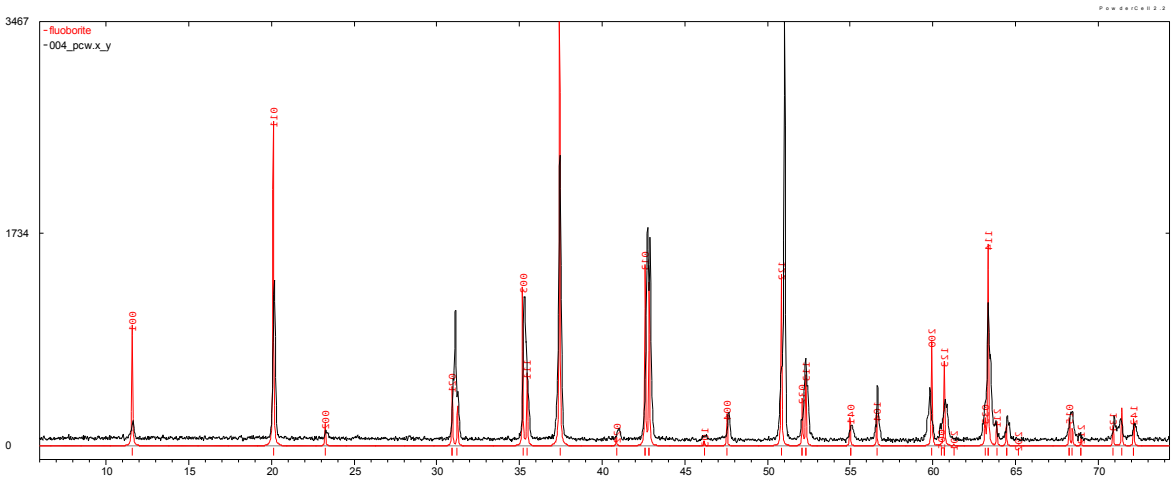

Figure S7. Experimental (black) and simulated (red) powder X-ray diffractograms for fluoborite sourced from Bodar Quarry, New Jersey, USA.

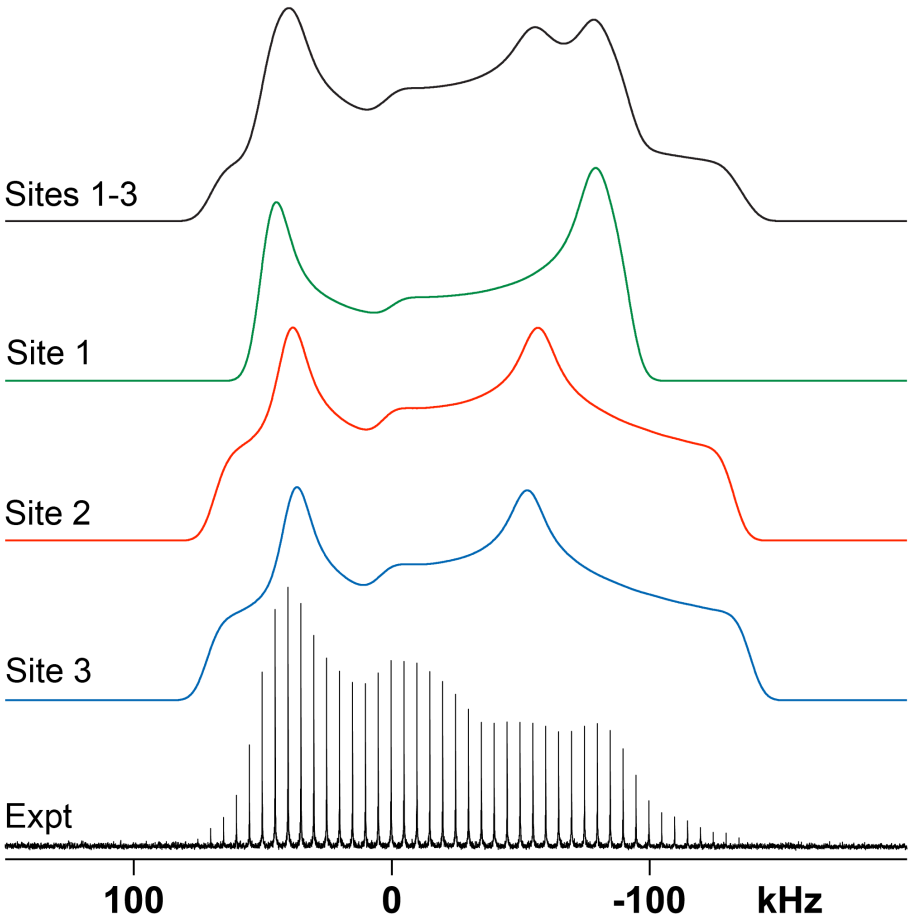

Figure S8. Experimental (lower trace: black) and simulated (upper traces: blue, red, green and black) ^{25}Mg NMR spectrum of boracite-Cl. Experimental NMR spectra acquired at B_0 = 21.1 T. Simulations were generated with WSolids using the NMR parameters listed in Table 1.

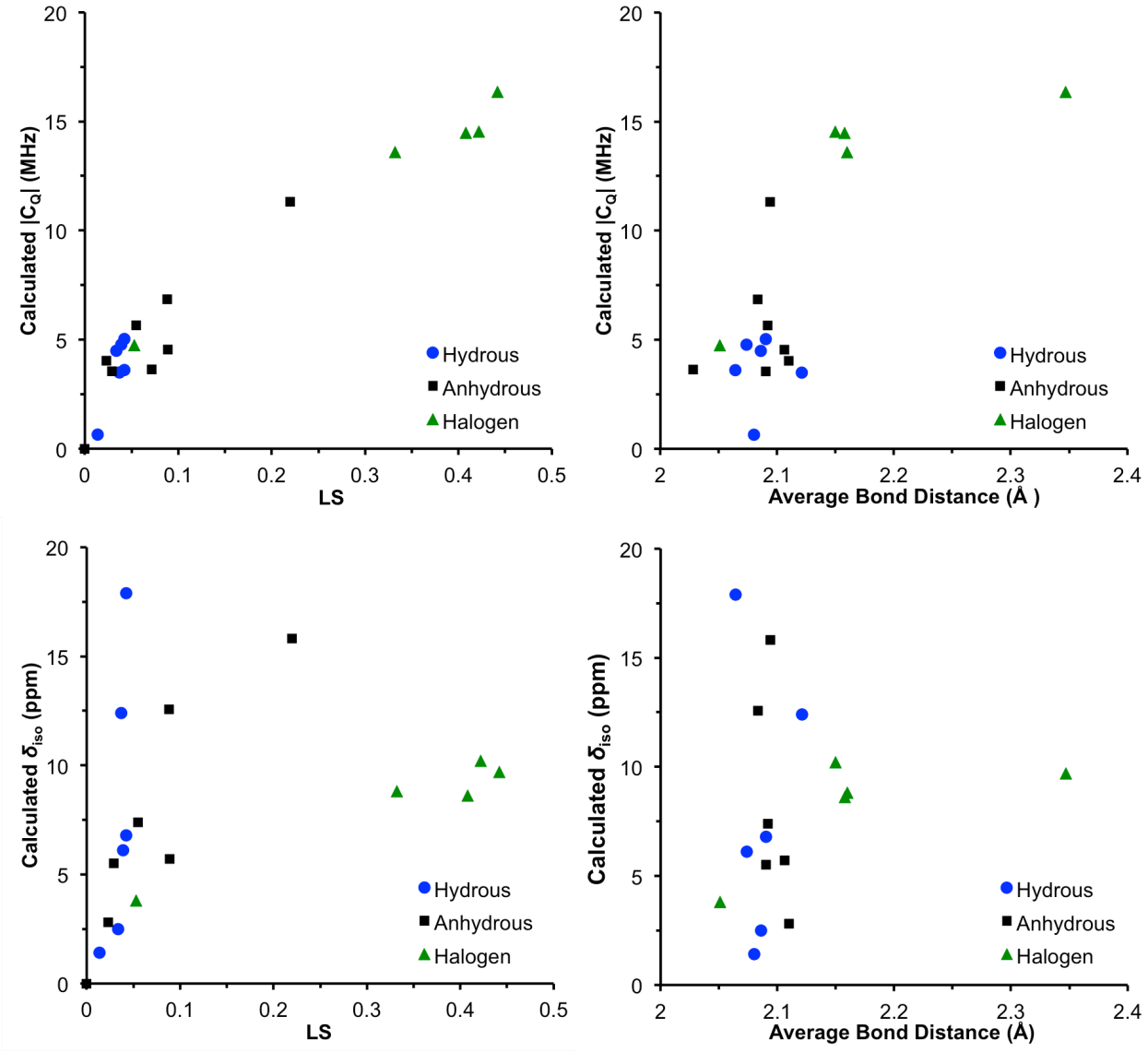

Figure S9. Plots of calculated ^{25}Mg C_Q or δ_{iso} values *vs* modified longitudinal strain (LS) or average bond distance between magnesium and its nearest neighbours. Values used are listed in Table 1.

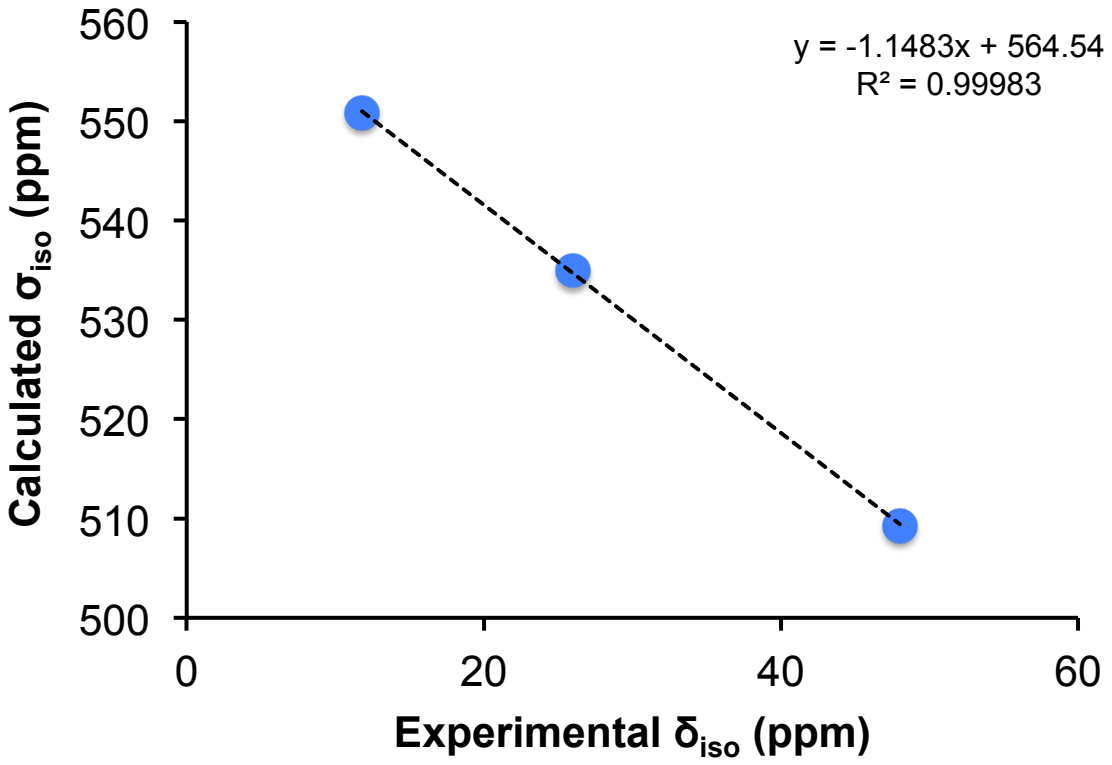

Figure S10. Relationship of experimental (δ_{iso}) and calculated (σ_{iso}) values of three reference compounds: brucite ($Mg(OH)_2$), periclase (MgO), and spinel ($MgAl_2O_4$). A linear regression analysis of these data reveal the following relationship $\delta_{iso} = -(\sigma_{iso} - 564.5$ ppm).

Quantum Chemical Calculations Background

In the case of insulator materials the effect of external magnetic field on the electron spin is usually small however not negligible.[1] The effect in this case is strictly related to the slight contraction and expansion of majority and minority spin wave functions under the external magnetic field. As a result nonzero spin density appears at the nucleus leading to in principle nonzero contact contribution for the NMR screening, known in metals. However, for studied here minerals such contribution to the shielding is constant and of only 10 ppm. Therefore considering NMR shift the essential contribution comes from the orbital motion of electrons, and the resulting induced current density ($\mathbf{j}_{ind}$) in most extend is the source of the screening. Therefore, following the Biot-Savart Law, the corresponding NMR shielding can be calculated theoretically on the basis of the following equations:[2-5]

$$\mathrm{B_{ind}(R)} = -\overleftrightarrow{\sigma}(\mathbf{R})\mathbf{B} = \frac{1}{c}\int \mathrm{d^3}\mathbf{r}\mathbf{j}_{ind}(\mathrm{r})\times\frac{\mathbf{R}-\mathbf{r}}{|\mathbf{r}-\mathbf{R}|^3}$$

where **B** is the external magnetic field, **r** and **R** are distance vectors, $\mathbf{B}_{ind}$ is the magnetic shielding field induced by the induced current ($\mathbf{j}_{ind}$) defined as:

$$\mathbf{j}_{ind}(\mathrm{r}') = \sum_o \left[\left\langle \Psi_o^{(1)}\middle|\mathrm{J}^{(0)}(\mathrm{r}')\middle|\Psi_o^{(0)}\right\rangle + \left\langle \Psi_o^{(0)}\middle|\mathrm{J}^{(0)}(\mathrm{r}')\middle|\Psi_o^{(1)}\right\rangle + \left\langle \Psi_o^{(0)}\middle|\mathrm{J}^{(1)}(\mathrm{r}')\middle|\Psi_o^{(0)}\right\rangle\right]$$

with ψ_o and ψ_e representing the ground and excited states, respectively, of the wavefunctions. The perturbed wavefunction is given by:

$$|\Psi_o^{(1)}\rangle = \sum_e \frac{|\Psi_e^{(0)}\rangle\langle\Psi_e^{(0)}|}{\epsilon - \epsilon_e}|\Psi_o^{(o)}\rangle$$

$$\mathrm{H}^{(1)} = \frac{1}{2c}\mathbf{r}\times\mathbf{p}\cdot\mathbf{B}$$

with $H^{(1)}$ as first-order perturbed Hamiltonian. After solving the wavefunctions, the magnetic shielding field and thus the magnetic shielding tensor at the nucleus can be calculated.

References

1. Laskowski, R.; Khoo, K. H.; Haarmann, F.; Blaha, P., Computational Study of Ga NMR Shielding in Metallic Gallides. *The Journal of Physical Chemistry C* **2017,** *121* (1), 753-760.
2. Laskowski, R.; Blaha, P., Origin of NMR Shielding in Fluorides. *Phys. Rev. B* **2012,** *85* (24), 245117.
3. Laskowski, R.; Blaha, P., Calculations of NMR Chemical Shifts with Apw-Based Methods. *Phys. Rev. B* **2012,** *85* (3), 035132.
4. Laskowski, R.; Blaha, P.; Tran, F., Assessment of Dft Functionals with NMR Chemical Shifts. *Phys. Rev. B* **2013,** *87* (19), 195130.
5. Laskowski, R.; Blaha, P., Understanding of ^{33}s NMR Shielding in Inorganic Sulfides and Sulfates. *J. Phys. Chem. C* **2015,** *119* (1), 731-740.